Understanding the high capacity of Li2FeSiO4: In situ XRD/XANES study combined with first-principles calculations

ARTICLE *in* CHEMISTRY OF MATERIALS · APRIL 2013

Impact Factor: 8.35 · DOI: 10.1021/cm303685p

CHEMISTRY OF MATERIALS

Article

pubs.acs.org/cm

Understanding the High Capacity of Li_2FeSiO_4: In Situ XRD/XANES Study Combined with First-Principles Calculations

Dongping Lv,[†] Jingyu Bai,[†] Peng Zhang,[‡] Shunqing Wu,[‡] Yixiao Li,[†] Wen Wen,[§] Zheng Jiang,[§] Jinxiao Mi,[▽] Zizhong Zhu,[‡] and Yong Yang*[,†]

[†]State Key Laboratory for Physical Chemistry of Solid Surfaces, College of Chemistry and Chemical Engineering, Department of Chemistry, Xiamen University, Xiamen, 361005, People's Republic of China

[‡]Department of Physics and Institute of Theoretical Physics and Astrophysics, Xiamen University, Xiamen, 361005, People's Republic of China

[§]Shanghai Synchrotron Radiation Facility, Shanghai Institute of Applied Physics, Chinese Academy of Sciences, Shanghai, 201204 People's Republic of China

[▽]Department of Materials Science and Engineering, College of Materials, Xiamen University, People's Republic of China

Supporting Information

ABSTRACT: The electrochemical mechanism of the cathode material Li_2FeSiO_4 with reversible extraction/insertion of more than one Li^+ from/into the structure has been studied by techniques of in situ synchrotron X-ray absorption near edge structure (XANES) and X-ray diffraction (XRD). These advanced techniques provide effective solutions to address the limitations of characterization by traditional ex situ methods. The study of in situ Fe K-edge XANES indicates that the Fe ion in the Li_2FeSiO_4 is oxidized continuously to high valence during the charging process from open circuit potential to 4.8 V, which contributes to the high reversible capacities of the materials. In situ XRD and theoretical study from first-principles calculations have been employed to reveal the structural evolution of the Li_2FeSiO_4 underlying the high capacity during the charge/discharge process. The results of both experimental and theoretical studies are consistent and indicate that Li_2FeSiO_4 undergoes two two-phase reactions when the electrode is charged to a high voltage of 4.8 V.

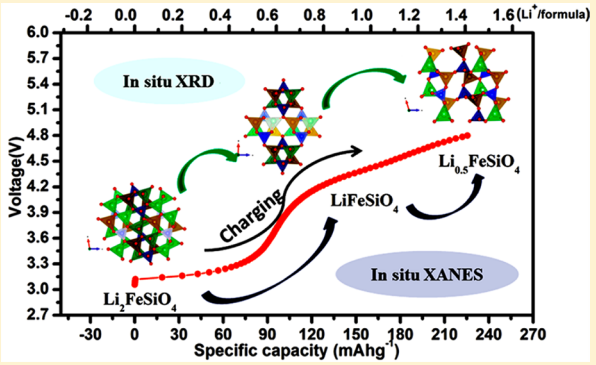

KEYWORDS: *lithium-ion battery, orthosilicate, cathode, synchrotron, electrochemistry, mechanism study, first principles calculation*

1. INTRODUCTION

Orthosilicate cathode materials (Li_2MSiO_4, M = Fe, Mn, etc.) in Li-ion batteries have attracted significant interest, because of their excellent safety characteristics, environmental benignity, and low cost.[1−6] Most importantly, Li_2MSiO_4 materials may realize two-electron exchange per formula to deliver a high theoretical capacity of ca. 330 mA h g^{-1}.[3] Among these orthosilicates, Li_2FeSiO_4 is particularly attractive, because of its outstanding electrochemical properties and complex polymorphism.[2,5,7−13] Pioneering work on Li_2FeSiO_4 has been undertaken both experimentally[2] and theoretically,[3] and, since then, great efforts have been made to optimize the materials by reducing particle size, applying a uniform carbon coating, optimizing phase and structure, and improving electrochemical performance.[10,14−19]

The charge/discharge of Li_2FeSiO_4 involved a multistep process, and until now, the mechanism of this process has not been fully understood. It is known that, upon reversible extraction/insertion of less than one Li^+ per formula unit, Li_2FeSiO_4 exhibits structural rearrangement, as suggested by the change of voltage plateau from 3.1 V to 2.8 V in the first and subsequent charge processes.[2,20] Nyten et al. found that, when Li_2FeSiO_4 in $Pmn2_1$ symmetry was charged to extract one Li^+ ion up to 3.8 V, the $LiFeSiO_4$ formed was isostructural with the pristine materials.[2] Through study of X-ray diffraction (XRD) and neutron diffraction on the cycled Li_2FeSiO_4, Armstrong et al. found that Li_2FeSiO_4 transformed from the $P2_1/n$ structure to the $Pmn2_1$ structure after cycling.[17] Ex situ XRD study was also carried out on charged Li_2FeSiO_4 by Kojima et al.; they found that, with the extraction of one Li^+, $LiFeSiO_4$ transformed to an ion-disordered (Li^+ and Fe^{3+}) new structure, which was isostructural with pristine Li_2FeSiO_4 in $P2_1/n$ symmetry.[21] These discrepancies in the observed mechanism may result from the differences in the sample polymorphs, because of different synthesis temperatures or preparation methods.[2,17,21]

Recently, we found that more than one Li^+ could be reversibly extracted from and inserted back into Li_2FeSiO_4 by

Received: November 14, 2012
Revised: April 21, 2013
Published: April 24, 2013

modifying the material structure,[11,22] which was also proved by other researchers.[15,23] However, the mechanism for that process, i.e., why and how more than one electron exchange could be achieved in Li_2FeSiO_4, is still unclear. This knowledge is essential for further optimizing the design and synthesis of this material. To address the issue, in situ synchrotron XRD and X-ray absorption near-edge structure (XANES) spectroscopy were performed to understand the charge/discharge mechanism of Li_2FeSiO_4, especially in the case of reversible extraction/insertion of more than one Li^+. In situ XANES was used to study the near-edge structure and valence evolution of the Fe ion during charge and discharge processes with multiple Li^+ ion reversible exchange, a direct proof of electron transfer on the Fe ion. At the same time, in situ XRD experiment was carried out to investigate the crystal structural evolution and phase transformation of the material, which relates closely to the electrochemical process of multiple-Li^+ reversible exchange. In addition, a computational study based on first principles was performed to further understand these observed experimental results from the in situ XANES and XRD.

2. EXPERIMENTAL SECTION

2.1. Synthesis of Li_2FeSiO_4/C Composite. The Li_2FeSiO_4/C composite was synthesized via a one-step solution−polymerization approach, as reported.[11] Typically, 0.01 mol of Fe powder and 0.02 mol of citric acid were mixed first in 30 mL of deionized water under vigorous magnetic stirring at 60 °C, resulting in white precipitation with the release of H_2. The resulted precipitation is gradually dissolved to form a clean jade-green ferrous citrate solution ∼10 h later. Stoichiometric amounts of tetraethyl orthosilicate (TEOS) (0.01 mol) and lithium acetate (0.02 mol) then were added into the solution and stirred for 4 h, where the solution still maintained its transparency. Then, 0.01 molof ethylene glycol was added into the solution and the oil bath temperature was increased to 130 °C and kept for 4 h for polymerization, yielding a viscous transparent polymer precursor. After drying at 80 °C for 24 h, the precursor was grounded into powder, pressed into pellet, and subsequently calcined in an argon atmosphere under preprogrammed heating process, i.e., the temperature was first increased to 400 °C at a rate of 2 °C min^{-1} and maintained for 5 h for the complete decomposition of organic groups, and then raised to 600 °C at the same speed and maintained for 10 h for the phase formation of Li_2FeSiO_4.

2.2. Construction of Electrochemical Cells for In Situ XRD and XANES Study. The in situ electrochemical cell fulfilling the transmission of X-rays was constructed on the base of a CR2032 coin cell. Briefly, two holes 2 mm in diameter were made at symmetrical positions of both cathode and anode shells, and then the holes were sealed well with Kapoton tape. The sealability, as well as the availability of the in situ cell, was confirmed to meet the requirements of the in situ electrochemical test. Slurry of the working electrode was prepared according to our previous work.[24] Initially, Li_2FeSiO_4 was mixed with acetylene black and poly(vinylidene fluoride) binder with a weight ratio 85:5:10, and then grounded by ball milling using *N*-methyl-2-pyrolidene as solvent. The mixture then was casted on aluminum net (current collector) and thereafter dried at 50 °C for 3 h under vacuum to obtain cathode. Finally, the in situ coin cells were assembled with prepared cathode, lithium anode, Celgard 2400 polypropylene separator, and 1 M $LiPF_6$ in ethylene carbonate/dimethyl carbonate (1:1 v/v) electrolyte. The charge/discharge performance of the Li_2FeSiO_4 during the in situ XRD and XANES tests was measured galvanostatically at various current densities in a voltage range of 1.5−4.8 V on a LAND CT-2001A battery test system (Wuhan, PRC) at room temperature. During the in situ XANES, the current density of coin cell was set to 15 mA g^{-1} for both charge and discharge processes. During the in situ XRD, the charge and discharge current densities were set to 10 and 20 mA g^{-1}, respectively.

2.3. Characterization. The structure of the samples was characterized by synchrotron radiation X-ray diffraction (XRD), using the BL14B1 beamline at the Shanghai Synchrotron Radiation Facility (SSRF) (Shanghai, PRC) and the wavelength of the X-ray employed is λ = 1.2398 Å. BL14B1 is a bending magnet beamline, and the storage ring energy of SSRF is 3.5 GeV. The beam was first collimated using a Rh/Si mirror and then monochromatized using a Si(111) double-crystal monochromator. After that, the beam was further focused by a Rh/Si mirror to the size of 0.5 mm × 0.5 mm. Higher-order harmonics were also rejected by the Rh/Si mirror. NaI scintillation detector was used for data collection.

The in situ XANES studies were performed at the BL14W1 beamline of SSRF and a Si (111) double-crystal monochromator, cooled by liquid nitrogen, was employed to monochromatize the energy. The measurements were performed using transmission mode. The XANES data were analyzed using the Athena program of IFEFFIT for background removal, absorption edge energy (E_0) determination and spectrum normalization, etc. Detailed information concerning the data processing of the XANES spectra and the definition of E_0 is included in the Supporting Information.

2.4. Theoretical Calculation. All calculations on Li_2FeSiO_4 compounds are based on density functional theory (DFT) and carried out by using the projector augmented wave method (PAW),[25] as implemented in the Vienna ab initio simulation package (VASP).[26] The exchange and correlation functional is treated as generalized gradient approximation (GGA) of the Perdew−Burke−Ernzerhof (PBE) formula.[27] The wave functions are expanded using the plane waves up to a kinetic energy cutoff of 500 eV. Brillouin-zone integrations are approximated by using special *k*-point sampling of Monkhorst−Pack scheme[28] with a *k*-point mesh resolution of $2\pi \times 0.03$ $Å^{-1}$. The unit-cell lattice vectors (unit cell shape and size) and atomic coordinates are fully relaxed until the force on each atom is <0.01 eV/Å. Furthermore, the effects that are due to the localization of d-electrons of the Fe ions in the silicates are also taken into account with the DFT + *U* approach.[29] Within this approach, an effective value of $U_{eff} = (U - J) = 4$ eV has been used. Such a value had been proved to be a close approximation for Fe^{2+}, Fe^{3+}, and Fe^{4+} in the silicate compounds.[30,31]

3. RESULTS AND DISCUSSION

The quality of the as-prepared Li_2FeSiO_4 was evaluated in powder form before in situ studies were performed. As shown by the synchrotron XRD pattern in Figure 1 a, the synthesized Li_2FeSiO_4 has no detectable Fe_2O_3 or Li_2SiO_3 impurities, those being the most commonly reported impurity phases, which is consistent with our previous result.[11] The product has a monoclinic $P2_1/n$ structure, which was discussed in our previous work,[11] and the refined lattice parameters are a = 8.2368(2) Å, b = 5.0235(7) Å, c = 8.2438(5) Å, β = 99.095(4)°, and V = 336.83 $Å^3$, with a figure-of-merit of $|\Delta 2\theta_{cal.-obv.}|$ = 0.0068(°) and $F(30)$ = 22.9 (172). Accordingly, XANES was also performed on the same sample, as shown in Figure 1b. It can be observed that the XANES spectrum of Li_2FeSiO_4 has an absorption edge at ∼7120 eV, which is similar to the profile of FeO. This indicates that the Fe ion in Li_2FeSiO_4 has a valence similar to that of the Fe ion in FeO. The stoichiometry of the reference compound FeO is verified to be $FeO_{1.013}$ by both gravimetric oxidation and thermogravimetric analysis, indicating a presence of ca. 2.6% Fe^{3+} in the compound (see the Supporting Information). The observed weak pre-edge peak at ∼7114 eV indicates the tetrahedral coordination of Fe ions in the crystal,[2] which is consistent with previous structural analysis.[32] The SEM observation demonstrates that the particles of Li_2FeSiO_4 are micrometer-sized with irregular shapes (see Figure S1a in the Supporting Information). However, on a higher magnification mode (Figure S1b in the

dx.doi.org/10.1021/cm303685p | *Chem. Mater.* 2013, 25, 2014−2020

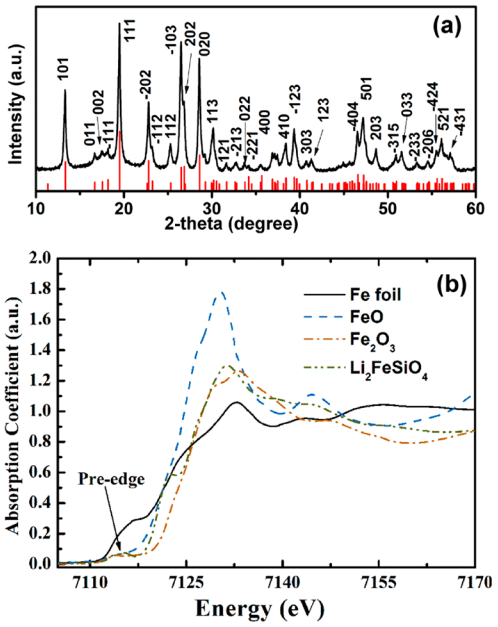

Figure 1. (a) Synchrotron XRD pattern and (b) XANES of powder Li_2FeSiO_4.

Supporting Information), it is observed that the large particles are composed of nanosized particles 40−50 nm in size, with spherical shape and uniform size distribution. Transmission electron microscopy (TEM) analysis (see Figure S1c in the Supporting Information) indicates that Li_2FeSiO_4 particles are connected tightly by carbon. High-resolution transmission electron microscopy (HRTEM) (Figure S1d in the Supporting Information) indicates that Li_2FeSiO_4 is crystalline and coated by carbon layer. Put together, these results indicate that our synthesized Li_2FeSiO_4 is comparable to the previous result[11] and, consequently, is suitable for the present in situ studies.

Figure 2 illustrates the charge/discharge profiles of the Li_2FeSiO_4 during the in situ XANES measurement. At

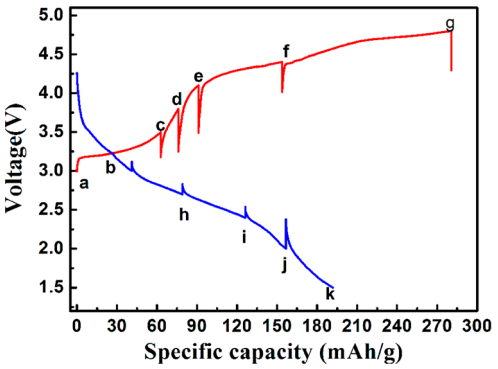

Figure 2. First charge/discharge profiles of Li_2FeSiO_4 at a current density of 15 mA g^{-1} between 1.5 V and 4.8 V during the in situ XANES measurement.

predetermined potentials during the charge/discharge process, marked "a"−"k", the galvanostatic process was halted and XANES spectra were collected after allowing the cell to rest for 30 min. From the charge/discharge curves (Figure 2), we can observe that, when cycled at a current density of 15 mA g^{-1}, the initial charge and discharge capacities are 280 and 195 mA h g^{-1}, respectively. This indicates that reversible exchange of more than one Li^+ is achieved in the system. The obtained high capacity benefits from the high-phase purity of the nanosized Li_2FeSiO_4 and its carbon composite structure. Because the nanosized particles of Li_2FeSiO_4 combined with in situ formed intimate conductive carbon layers decrease barrier to both Li^+ diffusion and charge transfer during the electrochemical reactions, which agrees well with previous results.[5,11,15,23]

The K-edge evolution of Fe ion in Li_2FeSiO_4 during first charge/discharge processes was studied by in situ XANES. XANES spectra of the reference compounds FeO and Fe_2O_3 were also collected under same experimental conditions and are presented in Figure 3. Before charging at open circuit potential

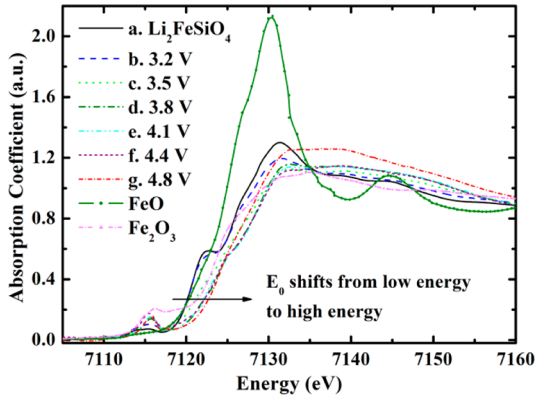

Figure 3. In situ Fe K-edge XANES spectra of Li_2FeSiO_4 electrode at different preset voltages during the charging process (a−g) and ex situ Fe K-edge XANES spectra of FeO and Fe_2O_3.

(OCP), the Li_2FeSiO_4 electrode has a XANES profile (Figure 3a) consistent with that of the powder sample (Figure 2b), indicating the suitability of both the electrode and the electrochemical cell for in situ study. The overlapped K-edges of Li_2FeSiO_4 and reference FeO suggest that the Fe ion in the majority of the Li_2FeSiO_4 has a valence of +2. When the Li_2FeSiO_4 electrode is charged to 3.2 V, with capacity of 30 mA h g^{-1}, no obvious shift in the K-edge of Fe is observed (Figure 3b). Similarly, with the charge capacity increased to 60 mA h g^{-1} when charged to 3.5 V (Figure 2c), the E_0 shift is also minimal (see Figure 3c). Based on the observed capacity of 60 mA h g^{-1} charged to 3.5 V, the calculated electron transfer on Fe^{2+} is ∼0.37 e per formula, which means that 37% of Fe^{2+} has transformed to Fe^{3+}. From comparison between the XANES spectra at OCP (Figure 3a), 3.2 V (Figure 3b), and 3.5 V (Figure 3c), there is an apparent change in the spectra shape of both the pre-edge and the white line. It is observed that the pre-edge peaks increase in intensity and become sharper in shape while the white line decreases, which is ascribed to valence increase of the Fe ion accompanying Li^+ extraction.[32] The observed results indicate that the E_0 shift, along with the voltages ranged from OCP to 3.5 V, has no linear relationship with the increasing charge capacity or the valence change of the Fe ion; thus, it is strongly suggested that a comprehensive evaluation of the entire XANES spectrum including the pre-edge feature, the E_0 shift, and the white line is essential to determine the valence change of the Fe ion, which was also suggested by other researchers.[33−35] The observed negligible E_0 shift but obvious change of both the pre-edge and white line during the charging from OCP to 3.5 V may be due to the special location of the Fe ion in a tetrahedral site in Li_2FeSiO_4.[33,34,36] When Li_2FeSiO_4 was charged to 3.8 V (a

dx.doi.org/10.1021/cm303685p | Chem. Mater. 2013, 25, 2014−2020

capacity of 75 mA h g^{-1}), there is a distinct E_0 shift, directly indicating an increase in the valence of the Fe ion. Charging to 4.1 V results in a small E_0 shift, which may be ascribed to the low charge capacity within the transitional period between two plateaus of 3.2 V and 4.5 V. A tremendous increase of the pre-edge is observed when charged to 4.4 V, which is accompanied by a charge capacity of 150 mA h g^{-1} and indicates continuous electrochemical oxidation of the Fe ions. Subsequent charging up to 4.8 V, with the increasing charge capacity, E_0 continuously shifts to higher energy, and that indicates a further valence increase of the Fe ions. Compared to the XANES spectrum of the reference compound Fe_2O_3, the Fe ion in the Li_2FeSiO_4 has higher E_0 energy than that of Fe_2O_3 when the electrode is charged to voltages above 4.1 V. This suggests that the Fe ion with a high valence of +4 is formed above the charging voltage of 4.1 V, which matches up with ex situ Mossbauer analysis and other reported results.[11,15,23]

In the discharge process, an inverse trend of the E_0 shift is observed for the Fe ion as Li^+ is intercalated back into the crystal structure (Figure 4). As shown in Figure 2, when

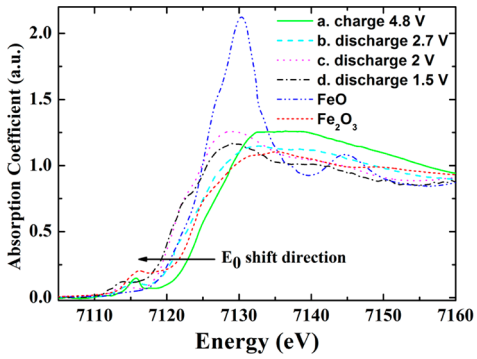

Figure 4. In situ Fe K-edge XANES of Li_2FeSiO_4 electrode at different preset voltages during the discharging process (a–d) and ex situ XANES spectra of FeO and Fe_2O_3.

Li_2FeSiO_4 is discharged to 2.7 V, a large amount of Li^+ (a capacity of 80 mA h g^{-1}) is inserted back into the structure; accompanying that, the E_0 of the Fe K-edge shifts to lower energy, indicating valence reduction during discharge. Compared to reference compounds, it is found that when Li_2FeSiO_4 is discharged to 2.7 V, the formed Fe^{4+} at the end of charge process is reduced to Fe^{3+} and then further reduced to Fe^{2+}. Discharged to 2 V, a continued E_0 shift to low energy is observed, indicating further reduction of the Fe^{3+} to Fe^{2+}. In the voltage range of 2–1.5 V, The observed discharge capacity is about 40 mA h g^{-1}. During that process, the E_0 shift is small, but an obvious pre-edge shift toward low energy is observed, which is in reverse trend, compared to the pre-edge shift in the preliminary stage of the charging process.

To summarize the E_0 evolution of the Fe K-edge during the charge and discharge processes, we compile the obtained E_0 values versus voltage and presented in Figure 5. As shown in Figure 5, as the voltage increases during charging, the E_0 of the Fe K-edge shifts to higher energy, indicating that continuous oxidation of the Fe ion accompanies extraction of Li^+ from the structure. At voltages above 4.1 V, the Fe ion has higher E_0 values than that of Fe_2O_3, suggesting the formation of Fe^{4+}. It should be mentioned here that the oxidation of O^{2-} in the crystal framework to form O^- or O_2 under high potential is also a possible route for charge balance of the electrode during the

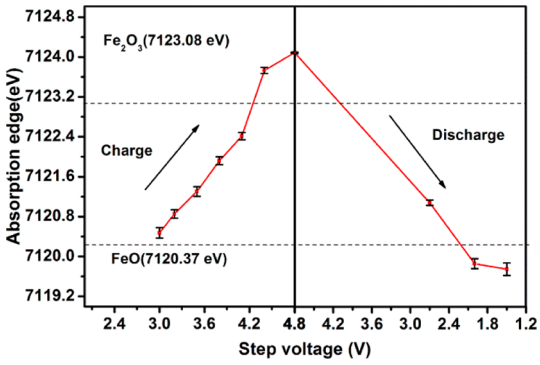

Figure 5. E_0 evolution of the Fe K-edge along with voltage change during charge and discharge processes.

charging process. However, this hypothesis can neither be supported nor excluded by the results of present work, and need further study on the state of oxygen during the charging process through soft X-ray XANES or other techniques. In the discharging process, the opposite trend of E_0 shift was observed, i.e., with decreasing discharge voltage, E_0 shifts back to a low energy, demonstrating the reduction of the Fe ion with intercalation of Li^+ back into crystal. When the electrode was discharged to 2 V and 1.5 V, the E_0 values of the Fe ion are lower than that of the reference compound FeO. Currently, we believe that may be caused either by the oxidation of our electrode in the preparation process or slightly oxidized reference compound FeO. As a matter of fact, that FeO is a typical nonstoichiometric compound,[37] and its actual stoichiometry is measured to be $FeO_{1.013}$ or $Fe(II)_{0.96}\,Fe(III)_{0.026}O$ by both gravimetric analysis and thermogravimetric analysis in the present study, indicating the presence of trace of Fe^{3+} in the reference compound (see the Supporting Information).

The above analysis from in situ XANES study suggests that it is the formation of Fe^{4+} when charged to high voltages above 4.1 V that accounts for the charge balance of the compound with reversible exchange of more than one Li^+ in the system. However, the relationship between the crystal structure and electrochemical properties, which is crucial to understanding the mechanism of charge/discharge and optimizing the structure of materials, is still unknown. Many efforts have been taken to understand the structural evolution of Li_2FeSiO_4 within one Li-ion extraction/insertion.[2,19−21] In the case of reversibly extracting more Li^+, however, mechanism study remains a challenge. Thus, in situ synchrotron XRD was carried out on the same electrode in the present work. Although real-time in situ XRD method is essential to the electrochemical mechanism study, the unavoidable weakened intensity of X-ray in penetrating the in situ cell usually results in decreased signal/noise ratio, especially from the diffraction of nanosized particles. Despite this, high-angle resolution synchrotron XRD provides sufficiently well-defined peak positions for evaluating phase changes during the reaction process.

During the in situ XRD study, the Li_2FeSiO_4 electrode exhibited similar electrochemical performance to during the in situ XANES study. As shown in Figure 6, initial charge and discharge capacities are 280 and 190 mA h g^{-1} at current densities of 10 and 20 mA g^{-1}, respectively, indicating that reversible extraction/insertion of more than one Li^+ is achieved. At the preset voltages (marked "a"–"l") during charging/discharging, the galvanostatic process was halted and XRD patterns were collected after allowing the cell to rest for 30 min.

dx.doi.org/10.1021/cm303685p | Chem. Mater. 2013, 25, 2014−2020

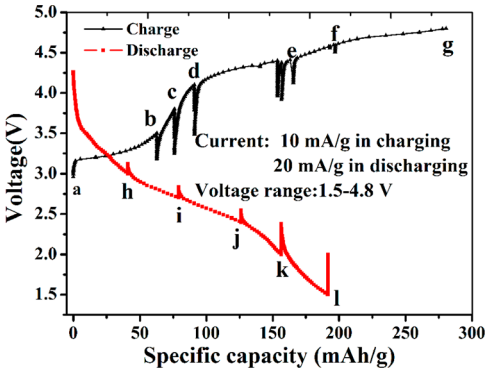

Figure 6. First charge/discharge profiles of Li_2FeSiO_4 at current densities of 10 mA g^{-1} (charging) and 20 mA g^{-1} (discharging) between 1.5 V and 4.8 V during the in situ XRD measurement.

It is noticed that the accumulation time of the first spectrum (trace "a" in Figure 7a) is 10 s per step, and that of other spectra are 30 s per step.

Accompanying continuous extraction of Li^+ during charging process, the crystal structure of Li_2FeSiO_4 experiences multistage evolution. Figure 7a shows the XRD patterns of the product at various charge voltages. At OCP before charging (trace "a" in Figure 7a), the Li_2FeSiO_4 electrode exhibits an XRD pattern quite similar to that of the Li_2FeSiO_4 powder sample (Figure 1a), but with decreased peak intensity; as in the powder sample, its peaks can be ascribed to the structure of monoclinic $P2_1/n$ (marked as α). The decreased peak intensity of the XRD pattern is caused by the barrier of the in situ cell and the transmission mode of XRD measurement. Charged to 3.5 V, with Li^+ extraction (a capacity of 65 mA h g^{-1}), the diffraction peaks from the pristine structure (α) are still visible; however, a new set of diffraction peaks is observed at low 2θ beside the 010, 011, and 210 peaks (trace "b" in Figure7a). These new peaks are ascribed to the structure of the charged $LiFeSiO_4$ phase (marked as β). In the subsequent charging process up to 4.1 V, peak intensity from the α structure decreases gradually; whereas that from the new β structure increases. This means that from OCP to 4.1 V, a two-phase transformation process from α to β happens, i.e., there is a reaction of Li_2FeSiO_4 (α) → $LiFeSiO_4$ (β) + Li^+ + e^-, which is consistent with the observation of the first voltage plateau at ~3.2 V. DFT investigation is performed to understand that reaction process and indicates that the formed β is isostructural to α (Figure 7b). The calculated pattern of phase β from DFT study is slightly different from that of phase α, and the peak shift to lower angle from α to β is due to the extraction of Li^+ from the structure, which is consistent with the experimental observation (Figure7a). Interestingly, when charged to a high voltage of 4.6 V, it is found that a very weak peak appears at a 2θ value of ~17° (trace "f" in Figure7a), and its peak intensity increases gradually during subsequent charging to 4.8 V. The new peak (marked as γ) may be ascribed to the diffraction from a new charged structure of Li_yFeSiO_4 ($0 \le y < 1$). Furthermore, in the voltage range of 4.1−4.8 V, a gradual decrease in diffraction intensity of the β phase accompanies the increasing intensity of the γ-phase. This suggests that there is another two-phase transformation process, as $LiFeSiO_4(\beta)$ → $Li_yFeSiO_4(\gamma)$ + $(1-y)Li^+$ + $(1-y)e^-$ ($0 \le y < 1$), in the voltage range of 4.1−4.8 V. This is consistent with the presence of the second charge plateau at ~4.5 V. It should be mentioned here that the phase transformation from $LiFeSiO_4$ (β) to Li_yFeSiO_4 (γ) is not

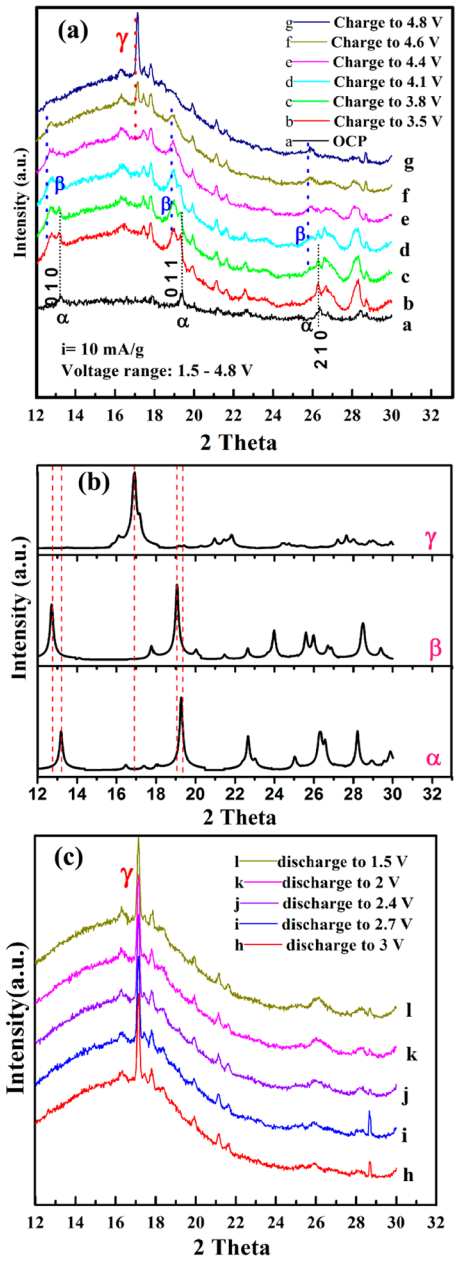

Figure 7. (a) In situ XRD patterns of Li_2FeSiO_4 electrode at different preset voltages during charging process (traces a−g); (b) computational XRD patterns of pristine Li_2FeSiO_4, charged $LiFeSiO_4$, and $Li_{0.5}FeSiO_4$; and (c) in situ XRD patterns of Li_2FeSiO_4 electrode at different preset voltages during discharging process (traces h and i).

complete in the present study, as evidenced by both the existence of weak diffraction from β at high potential and a reversible discharge capacity of <330 mA h g^{-1} (1.2 electron exchange per formula unit was achieved in present study). During the discharge process, negligible change is observed on the XRD patterns until a discharge voltage of 1.5 V (Figure 7b). The insignificant shift of the XRD peaks may be due to the weakened X-ray intensity by the in situ cell and amorphorization of material after charging process. We have also repeated that in situ XRD experiment by charging/discharging the cell without intermission during the XRD test, and obtained very similar result to the present study (see Figures S3 and S4 in the Supporting Information). Apparent phase transformation was observed in charging process; however, the data from the in situ

dx.doi.org/10.1021/cm303685p | Chem. Mater. 2013, 25, 2014−2020

XRD measurement are of insufficient quality to facilitate an accurate Rietveld XRD refinement.

To further understand the above experimental results especially the phase transformation, DFT calculations were carried out accordingly. Our calculations predict a phase transformation process from the pristine to cycled polymorphs of Li_2FeSiO_4 in the first charge process. For the pristine polymorph, the structure having a monoclinic $P2_1/n$ symmetry discussed in our previous work[11] is adopted for the calculations; whereas for the cycled polymorph, the site exchange of half of the Li ions and all of the Fe ions in the pristine Li_2FeSiO_4 structure is assumed, which is similar to the ion disordered (Li^+ and Fe^{3+}) structure reported by Kojima et al.[20] Based on the evolution of the in situ XRD patterns, the phase transformation processes are observed to occur accompanying the Li^+ extraction in the first charge process. The corresponding reactions are proposed and the average voltages are calculated, as shown in Table 1. According to reaction A, the calculated

Table 1. Proposed Reactions and Calculated Corresponding Average Voltages during the First Charge Process of Li_2FeSiO_4

	reaction	voltage (V)
A	Li_2FeSiO_4(pristine) ↔ $LiFeSiO_4$(charged) + Li	3.1
B	$LiFeSiO_4$(charged) ↔ $Li_{0.5}FeSiO_4$(cycled) + Li	4.3

voltage for the first Li^+ extraction is ca. 3.1 V, which is in good agreement with the experimental observation. The calculated XRD pattern of the charged $LiFeSiO_4$ (without Li−Fe antisite defects) is presented in trace β in Figure 7b for comparison. High consistency is observed between experimental and calculated XRD patterns, demonstrating high credibility of the theoretical prediction. When parts of the second Li^+ ions are further extracted, Li−Fe antisite defects takes place and the structure transfers from the charged $LiFeSiO_4$ to the cycled polymorph (reaction B), leading to a new cycled phase of $Li_{0.5}FeSiO_4$ (with Li−Fe antisite defects). Our results show that the cycled $Li_{0.5}FeSiO_4$ phase is stable, with respect to a two-phase mixture of $LiFeSiO_4$ and $FeSiO_4$, which may be formed during the electrochemical process. The calculated voltage of the reaction B is ca. 4.3 V, which is consistent with the experimental results. The calculated XRD pattern of such a $Li_{0.5}FeSiO_4$ is presented in trace γ in Figure 7b, which is consistent with our in situ XRD results with the appearance of diffraction peak ~17° (γ-phase in trace g in Figure 7a). In our previous study, we have also discovered ca. 1.4 Li^+ can be extracted reversibly from the Li_2FeSiO_4 structure,[11] which points approximately to the product of $Li_{0.5}FeSiO_4$. Crystal structures of these pristine Li_2FeSiO_4, charged $LiFeSiO_4$, and cycled $Li_{0.5}FeSiO_4$ are presented in Figure 8. For full extraction of the second Li ion, the calculated voltage is ca. 4.8 V with the volume expansion of the order of 20%, which indicates high barrier of the reaction.

4. CONCLUSION

The in situ XRD/XANES study and DFT calculations demonstrate that the two plateaus observed during charging of Li_2FeSiO_4 can be ascribed to two different two-phase transformation processes in the voltage ranges of OCP−4.1 V and 4.1−4.8 V, respectively. From OCP to 4.1 V, there is one two-phase reaction of $Li_2Fe(II)SiO_4(\alpha) \rightarrow LiFe(III)SiO_4(\beta) + Li^+ + e^-$, in which Fe ions are oxidized to Fe^{3+} and the crystal structure transforms to a charged $LiFeSiO_4(\beta)$. When the electrode is charged to voltages above 4.1 V, more Li^+ will be extracted through another two-phase reaction:

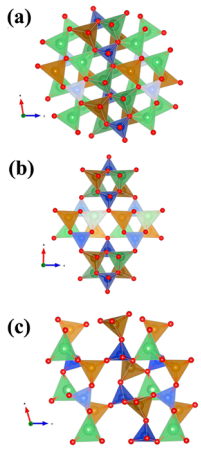

Figure 8. Crystal structures of (a) Li_2FeSiO_4, (b) $LiFeSiO_4$, and (c) $Li_{0.5}FeSiO_4$. [SiO_4 tetrahedrons are indicated in brown, FeO_4 tetrahedrons are indicated in blue, and LiO_4 tetrahedrons are indicated in green.]

$$LiFe(III)SiO_4(\beta) \rightarrow Li_yFe(III)_yFe(IV)_{1-y}SiO_4(\gamma) + (1-y)Li^+ + (1-y)e^- \quad (0 \le y < 1)$$

In that process, accompanying partial extraction of the second Li^+ from $LiFeSiO_4$, the Fe^{3+} is partially oxidized to Fe^{4+}, and the phase transforms from charged $LiFeSiO_4(\beta)$ to $Li_yFeSiO_4(\gamma)$ accordingly. After extraction of one Li^+ ion from the structure during the first charge, $LiFeSiO_4$ can maintain the same symmetry as that of pristine Li_2FeSiO_4 in $P2_1/n$. However, with the extraction of parts of the second Li ions from $LiFeSiO_4$, antisite defects occur between the Li and Fe ions, and the crystal structure rearranges to a new phase of Li_yFeSiO_4, where $y \approx 0.5$. These observations of the phase transformation are consistent with the results of first-principles study. The systematic study from both in situ XRD/XANES and DFT calculations provides new evidence to demonstrate the feasibility of exceeding one Li^+ reversible exchange in Li_2FeSiO_4 and suggests multiple phase transformation during the charge and discharge processes. This gives very good explanation about the observed high capacities of the materials in these previously reported publications. The study indicates that the orthosilicate Li_2FeSiO_4 can be developed as a potential high-capacity cathode material for next-generation Li-ion batteries.

■ ASSOCIATED CONTENT

Supporting Information

Supplementary figures of SEM, TEM, stoichiometry measurement of FeO, in situ XRD patterns obtained without intermission during charge and discharge processes, and data processing of XANES spectra. This material is available free of charge via the Internet at http://pubs.acs.org.

■ AUTHOR INFORMATION

Corresponding Author

*Tel.: +86-592-218-5753. E-mail: yyang@xmu.edu.cn.

Notes

The authors declare no competing financial interest.

■ ACKNOWLEDGMENTS

The financial supports from the National Natural Science Foundation of China (Grants Nos. 21233004, 21021002, 20873115 and 11004165), National Basic Research Program (973 Program, No. 2011CB935903) and General Motors (USA) are gratefully acknowledged. The synchrotron radiation XRD and XANES were performed at beamlines BL14B1 and BL14W, respectively, at the Shanghai Synchrotron Radiation Facility (SSRF) (Shanghai, China). We thank Mikhail Gordin from the Pennsylvania State University for helping to revise the writing of this paper.

■ REFERENCES

(1) Zaghib, K.; Simoneau, M.; Choquette, Y.; Armand, M. Canadian Patent CA 2200998 1997.
(2) Nyten, A.; Abouimrane, A.; Armand, M.; Gustafsson, T.; Thomas, J. O. *Electrochem. Commun.* **2005**, *7* (2), 156.
(3) Arroyo-de Dompablo, M. E.; Armand, M.; Tarascon, J. M.; Amador, U. *Electrochem. Commun.* **2006**, *8* (8), 1292.
(4) Goodenough, J. B.; Kim, Y. *Chem. Mater.* **2010**, *22* (3), 587.
(5) Islam, M. S.; Dominko, R.; Masquelier, C.; Sirisopanaporn, C.; Armstrong, A. R.; Bruce, P. G. *J. Mater. Chem.* **2011**, *21* (27), 9811.
(6) Gong, Z.; Yang, Y. *Energy Environ. Sci.* **2011**, *4* (9), 3223.
(7) Dominko, R. *J. Power Sources* **2008**, *184* (2), 462.
(8) Gong, Z. L.; Li, Y. X.; He, G. N.; Li, J.; Yang, Y. *Electrochem. Solid-State Lett.* **2008**, *11* (5), A60.
(9) Nishimura, S. I.; Hayase, S.; Kanno, R.; Yashima, M.; Nakayama, N.; Yamada, A. *J. Am. Chem. Soc.* **2008**, *130* (40), 13212.
(10) Boulineau, A.; Sirisopanaporn, C.; Dominko, R.; Armstrong, A. R.; Bruce, P. G.; Masquelier, C. *Dalton Trans.* **2010**, *39* (27), 6310.
(11) Lv, D. P.; Wen, W.; Huang, X. K.; Bai, J. Y.; Mi, J. X.; Wu, S. Q.; Yang, Y. *J. Mater. Chem.* **2011**, *21* (26), 9506.
(12) Wu, S. Q.; Zhu, Z. Z.; Yang, Y.; Hou, Z. F. *Comput. Mater. Sci.* **2009**, *44* (4), 1243.
(13) Zaghib, K.; Salah, A. A.; Ravet, N.; Mauger, A.; Gendron, F.; Julien, C. M. *J. Power Sources* **2006**, *160* (2), 1381.
(14) Zhang, S.; Deng, C.; Yang, S. Y. *Electrochem. Solid-State Lett.* **2009**, *12* (7), A136.
(15) Muraliganth, T.; Stroukoff, K. R.; Manthiram, A. *Chem. Mater.* **2010**, *22* (20), 5754.
(16) Sirisopanaporn, C.; Boulineau, A.; Hanzel, D.; Dominko, R.; Budic, B.; Armstrong, A. R.; Bruce, P. G.; Masquelier, C. *Inorg. Chem.* **2010**, *49* (16), 7446.
(17) Armstrong, A. R.; Kuganathan, N.; Islam, M. S.; Bruce, P. G. *J. Am. Chem. Soc.* **2011**, *133* (33), 13031.
(18) Kojima, T.; Kojima, A.; Miyuki, T.; Okuyama, Y.; Sakai, T. *J. Electrochem. Soc.* **2011**, *158* (12), A1340.
(19) Sirisopanaporn, C.; Masquelier, C.; Bruce, P. G.; Armstrong, A. R.; Dominko, R. *J. Am. Chem. Soc.* **2011**, *133* (5), 1263.
(20) Nyten, A.; Kamali, S.; Haggstrom, L.; Gustafsson, T.; Thomas, J. O. *J. Mater. Chem.* **2006**, *16* (23), 2266.
(21) Kojima, A.; Kojima, T.; Sakai, T. *J. Electrochem. Soc.* **2012**, *159* (5), A525.
(22) Lv, D.; Huang, X.; Wen, W.; Li, Y.; Yang, Y. *ECS Meet. Abstr.* **2010**, *1003* (1), 497.
(23) Rangappa, D.; Murukanahally, K. D.; Tomai, T.; Unemoto, A.; Honma, I. *Nano Lett.* **2012**, *12* (3), 1146.
(24) Lv, D. P.; Huang, X. K.; Yue, H. J.; Yang, Y. *J. Electrochem. Soc.* **2009**, *156* (11), A911.
(25) Blöchl, P. E. *Phys. Rev. B* **1994**, *50* (24), 17953.
(26) Kresse, G.; Furthmüller, J. *Comput. Mater. Sci.* **1996**, *6* (1), 15.
(27) Perdew, J. P.; Burke, K.; Ernzerhof, M. *Phys. Rev. Lett.* **1996**, *77* (18), 3865.
(28) Monkhorst, H. J.; Pack, J. D. *Phys. Rev. B* **1976**, *13* (12), 5188.
(29) Dudarev, S. L.; Botton, G. A.; Savrasov, S. Y.; Humphreys, C. J.; Sutton, A. P. *Phys. Rev. B* **1998**, *57* (3), 1505.
(30) Wang, L.; Maxisch, T.; Ceder, G. *Phys. Rev. B* **2006**, *73* (19), 195107.
(31) Zhang, P.; Hu, C. H.; Wu, S. Q.; Zhu, Z. Z.; Yang, Y. *Phys. Chem. Chem. Phys.* **2012**, *14*, 7346.
(32) Dominko, R.; Arcon, I.; Kodre, A.; Hanzel, D.; Gaberscek, M. *J. Power Sources* **2009**, *189* (1), 51.
(33) Bianconi, A.; Fritsch, E.; Calas, G.; Petiau, J. *Phys. Rev. B* **1985**, *32* (6), 4292.
(34) Balasubramanian, M.; Melendres, C. A.; Mini, S. *J. Phys. Chem. B* **2000**, *104* (18), 4300.
(35) Asada, E. *Chem. Lett.* **1974**, *3* (12), 1467.
(36) Bocquet, A. E.; Fujimori, A.; Mizokawa, T.; Saitoh, T.; Namatame, H.; Suga, S.; Kimizuka, N.; Takeda, Y.; Takano, M. *Phys. Rev. B* **1992**, *45* (4), 1561.
(37) Greenwood, N. N.; Earnshaw, A. *Chemistry of the Elements*, 2nd Edition); Elsevier Science & Technology Books: Amsterdam, 1997.